Influence of metallic matrix on erosion-corrosion behaviour of high chromium cast irons under slurry impingement conditions

L. Giourntas[a], F. Brownlie[a,b], T. Hodgkiess[a,c], A. M. Galloway[b]

[a] Weir Advanced Research Centre, Glasgow, UK

[b] Department of Mechanical & Aerospace Engineering, University of Strathclyde, Glasgow, UK

[c] School of Engineering, University of Glasgow, UK

Abstract

Chromium cast irons (CCI) comprise versatile materials that encompass a range of compositions and microstructures often chosen to promote good wear resistance. There are, however, issues that arise when the cast iron is required to operate in conditions where corrosion, as well as, wear is a factor. This scenario usually results in adapting the composition of the CCI in order to achieve higher chromium content in the metallic matrix and, thereby, to attain the corrosion resistance exhibited by high-Cr stainless steels. This paper comprises a comparison of the corrosive wear behaviour of an austenitic-based hypoeutectic cast iron and a martensitic-based, near-eutectic cast iron with the associated stainless steels, in a saline water under solid-liquid submerged jet conditions. A comprehensive experimental methodology has been adopted including evaluation of the behaviour of the materials in free erosion-corrosion conditions and with the application of cathodic protection. This approach has extended the understanding of the fundamental deterioration mechanisms in different hydrodynamic conditions and has highlighted the complexities of the mechanical/electrochemical interactions occurring during erosion-corrosion. An important feature is the influence of micro-galvanic interactions at phase boundaries. The impact of the findings has been discussed in terms of CCI alloy selection and corrosion control strategies.

1. Introduction

Chromium cast irons (CCIs) are commonly used for high wear applications such as slurry pumps and minerals processing equipment. The degree of damage of mechanical, electrochemical and interaction mechanisms in the mining supply chain governs the selection of the cast iron material type. Most alloy development has focused on increasing the wear resistance by variations of the casting technology (e.g. sand casting and centrifugal casting) and the incorporation of harder carbides into the white chromium cast iron structure but there is also interest in modification of its metallic matrix to mimic the superior corrosion resistance of the stainless steels.

CCIs comprise of three key elements; iron, chromium and carbon and, to that extent, they are rather similar to stainless steels. The major difference between these two classes of material is the much higher carbon content of the cast irons which, on account of the high affinity between chromium and carbon, provokes the precipitation of hard, chromium-containing, carbides. In both classes of alloys, the presence of chromium is also important in enhancing the corrosion resistance of the metallic matrix. In cast irons, the carbides are present in the form of relatively-fine eutectic dispersions in association with either an iron-rich metallic matrix (so-called hypoeutectic cast iron) or in the interstices between coarse dendrites of carbide – hypereutectic structure. The eutectic composition, although slightly dependent upon overall alloy composition, is around 3%C. For service in corrosive slurries, most of the commercially-used CCIs are of the hypoeutectic variant because the other type is often deficient in toughness and corrosion resistance [1]. Increasing the carbon content raises the volume fraction of carbides (CVF) considerably and this provides an improvement in the abrasive wear resistance of the cast irons, as it raises their bulk hardness and leads to lower inter-carbide spacing that is also an important factor of the cast iron performance under abrasive wear [2, 3]. Another option, to potentially improve the abrasive wear resistance of white cast irons, is by incorporating elements with a relatively high affinity to carbon. Additions of titanium [4, 5], niobium [6, 7] and mixed carbide formers [8] have been found to improve abrasive wear resistance of white cast irons as a result of producing refinement of the carbides – in some cases [5, 7] involving altering the cast iron structure from hypereutectic to the hypoeutectic form. Similar improvements in sliding wear resistance (but not in terms of dry erosion performance) have been observed [8] when utilising mixed (boron, vanadium, niobium, tungsten) carbide formers.

In terms of erosion and erosion-corrosion behaviour of white cast irons, there are no simple relationships between carbide volume fraction (CVF) and material loss. For instance, in dry erosion conditions, the wear-rate/CVF relationships have been found [9] to be critically dependent upon the type and particle size of the erodent and the impingement velocity. In corrosion and erosion-corrosion conditions, the relative performances of CCIs appears to be associated with the CVF, matrix chromium concentration [10] and Cr:C ratio [11] but has also been found [1, 12, 13] to depend upon the relative dominance of mechanical damage and corrosive attack. The approach adopted by Neville et al. [14, 15] involved assessing the ratio of the chromium concentration in the carbides and matrix ($Cr_{carbides}/Cr_{matrix}$), to quantify the corrosion performance of white cast irons in static, flowing and solid-liquid conditions. They

found that the lower the $Cr_{carbides}/Cr_{matrix}$ ratio, the better the corrosion resistance that would be obtained.

Another important feature, in relation to the corrosion and corrosive wear resistance of chromium cast irons, is the fact that the metal matrix and carbides exhibit different equilibrium corrosion potentials. The relevance of the associated galvanic interactions, as contributors to the synergy component to overall material loss, has been demonstrated or discussed by a number of investigators [16-20].

Over the past years, many researchers have compared different types of white cast irons primarily with steels and stainless steels, in relation to their corrosion, erosion and erosion-corrosion behaviour. Some studies have observed the superior corrosive wear properties of the white cast irons [13, 21, 22] although the comparative performances have been observed to depend upon impingement angle [23, 24], impinging-particle size [15] and impingement velocity/particle loading [25].

In summary, the first consideration, in the aim to produce satisfactory performance of CCIs in erosion-corrosion environments, is to develop a microstructure that contains chromium carbides in appropriate dispersions in an alloy matrix that contains sufficient Cr to impart corrosion resistance. An additional factor, however, is to take account of the influence of mechanical and corrosion interactions that are a feature of corrosive wear deterioration. Thus, the objective of the present work was to investigate the complex deterioration mechanisms that occur within two hypoeutectic high chromium white cast irons with different %C and %Cr contents (Fe-27Cr-3C and Fe-37Cr-1.8C) in two hydrodynamic zones. Properties like the CVF factor, bulk hardness and the Cr/C ratio were investigated through submerged slurry impingement tests. The corrosion component, based on the $Cr_{matrix}/Cr_{carbides}$ ratio of each white cast iron was also evaluated, through potentiodynamic polarisation scans. In addition to the cast irons, the experimental programme included an austenitic (UNS S31600) and a martensitic (UNS S42000) stainless steel with microstructures that mimic the desired properties of CCIs in terms of wear resistance obtained from a martensitic stainless steel and the corrosion resistance provided by an austenitic stainless steel. The test materials in this study are the same as those which were previously evaluated in a study assessing the effect of pH under corrosive wear conditions [13].

An in-house developed technique [26] facilitated the quantification of the impingement erosion, sliding abrasion, corrosion and the synergy effects of the deterioration mechanisms of the investigated materials.

2. Materials & Methods

The alloys that were selected for this study are listed below:

- A near-eutectic, hypoeutectic chromium cast iron Fe-27Cr-3C alloy, referred as 27%Cr cast iron herein, which possess good wear resistance and low/moderate corrosion resistance through a eutectic structure derived from hard M_7C_3 type carbides and high hardness martensitic matrix.
- The hypoeutectic cast iron, named as 37%Cr cast iron herein, which yields improved corrosion resistance by reducing the amount of chromium carbides and maintaining more chromium in the matrix, transforming to austenite, to attain the corrosion resistance associated with the 300 series austenitic stainless steels but with improved wear resistance.
- Austenitic stainless steel (UNS S31600), which exhibits good corrosion resistance in various corrosive environments.
- Martensitic stainless steel (UNS S42000), which has higher strength/hardness but moderate corrosion performance in saline conditions.

Table 1 illustrates the nominal compositions of the test materials, provided by the suppliers. Table 2 demonstrates the materials' densities along with their measured macro-hardnesses.

Table 1: *Nominal composition (wt%) of the stainless steels and cast irons*

Material	C	Cr	Ni	Mo	S	Mn	Si	N	P	Fe
UNS S31600	≤0.08	16-18	10-14	2.0-3.0	≤0.03	≤2.0	≤0.75	≤0.1	0.045	Bal.
UNS S42000	<0.15	12-14	-	-	<0.03	<1	<1	-	<0.04	Bal.
27%Cr cast iron	3.0	27	-	-	-	-	-	-	-	Bal.
37%Cr cast iron	1.8	37	-	-	-	-	-	-	-	Bal.

Table 2: *Nominal densities and measured hardness of the stainless steels and cast irons*

Material	Density (g/cm^3)	Hardness (HV-5kgf)
UNS S31600	8.00	200
UNS S42000	7.85	280
27%Cr cast iron	7.50	765
37%Cr cast iron	7.65	365

Figures 1a and 1b illustrate the microstructures of the 27%Cr and 37%Cr cast irons respectively through their cross sections. The 27%Cr cast iron has eutectic M_7C_3 rod-type chromium carbides (white) with eutectic martensite (light brown) and primary martensite (dark brown). This microstructure occurs as a result of the post-casting heat treatment to transform the as-cast, primary austenite to hard martensite and also produces secondary carbides. On the other hand, 37%Cr cast iron consists of austenitic dendrites and eutectic structure of austenite and small size (around 1-2μm) $M_{23}C_6$ chromium carbides. The average size of the chromium carbides in 27%Cr cast iron is larger than compared to the chromium carbides in 37%Cr cast iron, as a result of their different solidification processes.

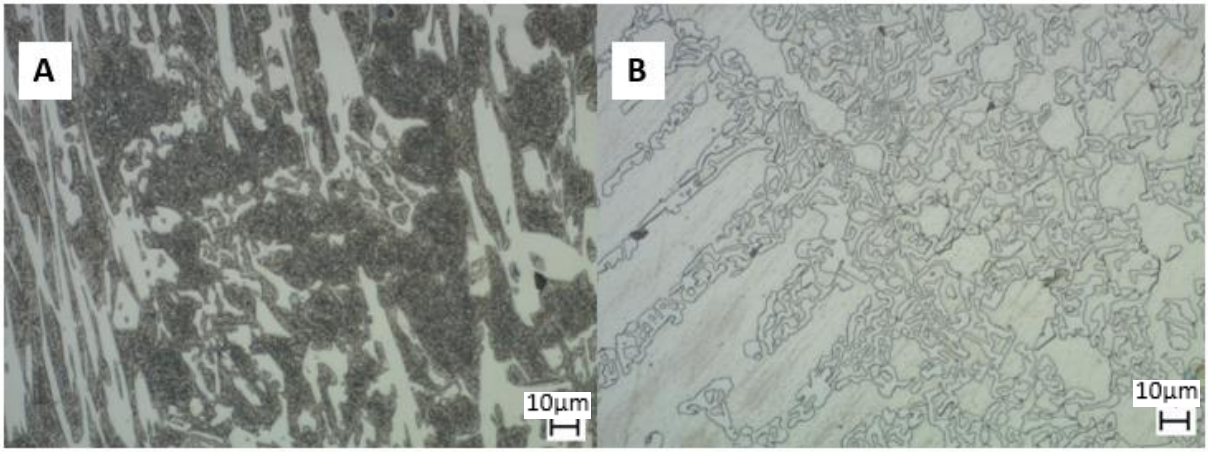

Figure 1: *Microstructure of a) 27%Cr cast iron with the large size eutectic carbides and eutectic and primary martensite; b) 37%Cr cast iron with the eutectic structure and austenite dendrites [26]*

The erosion-corrosion experiments were carried out using a circulating closed-loop rig, employing submerged-jet impingement, described previously [27]. The nozzle diameter of the impinging jet was 4 mm. The tests were carried out in a slurry comprising aqueous solution with 3.5% NaCl and 0.2 kg/m^3 sand particles, impinged at 17 m/s velocity perpendicular to the specimen surface (38mm dia.). The angular silica sand particles were of size range 250-700μm [25] with hardness of about 1160HV. The experiments were conducted at a temperature of 39±1ºC and the testing duration was 2h. All test samples were ground to 1200grit SiC prior to testing. After the free erosion-corrosion experiments, the martensitic stainless steel (UNS S42000) and the 27%Cr cast iron were immersed briefly in an inhibited acid solution (Clark's solution) in order to remove the extensive corrosion products on their surface prior to weighing. The austenitic stainless steel and the 37%Cr cast iron, on the other hand, exhibited negligible

corrosion product on their post-test surface. The solid-liquid impingement tests were conducted under both free-erosion corrosion conditions (FEC) and also with impressed current cathodic protection in order to provide information on the material degradation mechanisms occurring on the tested materials.

In-situ potentiodynamic scans were conducted to assess the electrochemical corrosion rates in solid-liquid impingement conditions. The potentiodynamic scans were conducted 15 min after the sample was submerged to allow for the free corrosion potential, E_{corr}, to stabilise. Gill AC electrochemical monitoring equipment was utilised for the potentiodynamic polarisation and cathodic protection tests. Platinum was used for the auxiliary electrode and Ag/AgCl employed as the reference electrode. Anodic polarisation tests were conducted by shifting the initial electrode potential 20 mV more negative than the free corrosion potential, hence ensuring that the transition point would occur. Scans were then made as far as 300 mV more positive at a sweep rate of 15 mV/min. The chosen ranges were sufficient to evaluate corrosion current measurements by way of Tafel extrapolation. The measured current densities were then used to calculate the associated mass losses due to corrosion using Faraday's Law. To conduct the polarisation tests, an electrically conductive wire was connected to the rear of the specimens, which were then cold mounted in epoxy resin. To obtain a better understanding of the electrochemical processes which occur on each wear region (Direct Impinged Zone – DIZ and outer area – OA), anodic polarisation scans were also undertaken on segmented specimens. The segmented specimen comprised of two separate samples; first a 7mm hole was water-jet cut in the centre of a 38mm diameter specimen. Into this hole a 5mm diameter sample, which represents the DIZ, was inserted and electrically isolated from the remainder of the specimen by a heat shrink polymer tube and epoxy resin. Electrical connecting wires were attached to the back of each specimen and then encapsulated by a cold mounting procedure [26]. For the cathodic protection experiments, the electrode potential was maintained at −800 mV (Ag/AgCl) at which potential back extrapolation of the anodic polarisation curves demonstrated that residual anodic reaction rates were negligible. Cathodic polarisation tests (down to -900 mV (Ag/AgCl) on these alloys have been reported elsewhere [28] and show no evidence of overprotection.

Post-test analysis was also conducted using an Alicona Infinite Focus 3D optical profilometer with a wear scar volume accuracy of ± 0.02mm^3. The 3D surface topography enabled a quantification of the material loss in the DIZ and OA regions which occur on the test samples,

as demonstrated in Figure 2. Post-test surface and sub-surface images were observed using a Hitachi SU-6600 SEM with a 20kV accelerating voltage, which was also used for quantitative analysis of the chromium content in the cast irons through wavelength dispersive X-ray Spectroscopy (WDS). A Mitutoyo MVK-G1 micro-hardness testing machine with 50gf load was used to measure the hardness of the chromium carbides of the white cast irons and the primary metallic phases (austenite and martensite). A Zwick ZHVI Knoop hardness test machine was used to measure the subsurface hardening effect on the post-test surface of the austenitic stainless steel. The load for each indention was 500gf and the distance between each indentation was kept greater than 270μm.

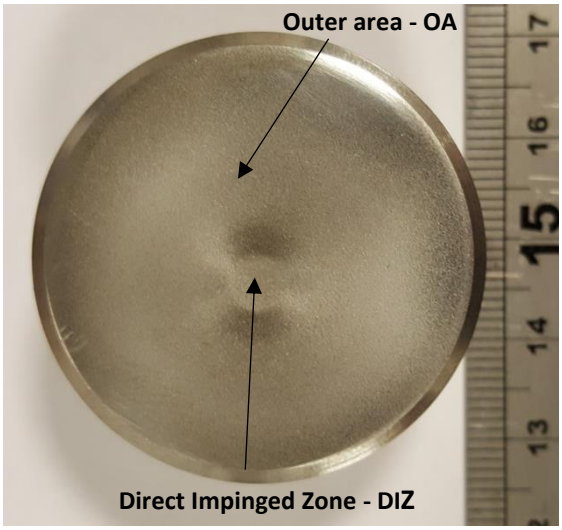

Figure 2: *Example of post-test sample with different wear regions*

3. Results & Discussion

3.1 Chromium concentration ratio and micro-hardness measurements

WDS was utilised to quantify the %Cr content in the matrix and the carbides of the two white irons. Table 3 shows the average values of measured chromium contents of the metallic matrix and the chromium carbides out of three replicates and the ±1 represents their scatter. The obtained chromium contents of the matrix distinguish clearly the martensitic structure of the 27%Cr cast iron and the austenitic structure of the 37%Cr cast iron. The $Cr_{carbides}/Cr_{matrix}$ ratio has also been calculated as it determines the corrosion resistance of the white cast irons.

Table 3: *WDS point analysis (wt%) of the two white cast irons*

Alloy	Cr_{matrix}	$Cr_{carbides}$	$Cr_{carbides}/Cr_{matrix}$
27%Cr cast iron	14.6 ± 1	52.1 ± 1	3.6

37%Cr cast iron	23.5 ± 1	60.7 ± 1	2.6

Table 4 illustrates the volume fractions of the three different constituents of each cast iron, which were determined by Image J analysis of the materials' cross sections.

Table 4: *Volume fractions of the different phases of the composite-like microstructure of cast irons*

27%Cr cast iron	**Average volume fraction (%)**	**37%Cr cast iron**	**Average volume fraction (%)**
Primary martensite	39	Austenite Dendrites	57
Eutectic Martensite	34	Eutectic austenite	27
Eutectic Carbides	27	Eutectic Carbides	16
Total	100	Total	100

The micro-hardness test technique also enhances the understanding of the erosion mechanisms that take place on each cast iron, as it is well known that the carbides are wear resistant in comparison with the metallic matrix which is likely to erode preferentially under slurry. Hence, an average of ten micro-hardness measurements was conducted on the primary solidification phase, eutectic structure, and the chromium carbides as shown in Table 5. Due to the small size of the eutectic carbides of the 37%Cr cast iron, their micro-hardness could not be measured directly and were estimated through the rule of mixtures. The measured/estimated hardness values of the chromium carbides are in agreement with the literature, where the H_{Cr7C3} is reasonably near to 1200HV [1] and the H_{Cr23C6} is about 976HV [29].

Table 5: *Micro-hardness values of the different phases of the composite-like microstructure of cast irons*

Material	**Primary solidification phase (50gf)**	**Eutectic Structure (200gf)**	**Eutectic Carbides (50gf)**
27%Cr cast iron	640 HV	733 HV	1114 HV
37%Cr cast iron	251 HV	459 HV	968HV

3.2 Volume loss measurements

Figure 3 illustrates the average volume losses of the comparative materials with error bars representing the scatter band from three replicates under free erosion-corrosion (FEC) and also

with the application of cathodic protection (CP). It is evident that the performance of all materials under FEC conditions was similar. According to the cathodic protection results, the 27%Cr cast iron exhibits superior erosion performance compared to the other comparative materials. The martensitic stainless steel follows the 27%Cr cast iron erosion behaviour and the UNS S31600 stainless steel is comparable to the 37%Cr cast iron. These results are not in accordance with some previous studies, which have reported that the erosion-corrosion resistance of white cast irons is superior to that of stainless steels [13, 21, 22]. However, these previous studies involved different testing conditions; e.g. much higher solid loadings, which would tip the test conditions into the erosion-dominant regime. This aspect received attention in, a solid/liquid impingement study [25], conducted in the authors' laboratory, which examined the effect of higher erosivity of the slurry (higher velocity and sand loading) and indeed demonstrated the superiority of these two cast irons over the stainless steels. This again indicates how the material performance under erosion-corrosion conditions is crucially dependent on the balance between mechanical and electrochemical severity which has also been noted by others [17]. This feature, of the martensitic-based alloys exhibiting superior resistance compared with the austenitic-based materials under mechanically-dominant conditions, was also demonstrated in the results obtained during the application of CP (Figure 3).

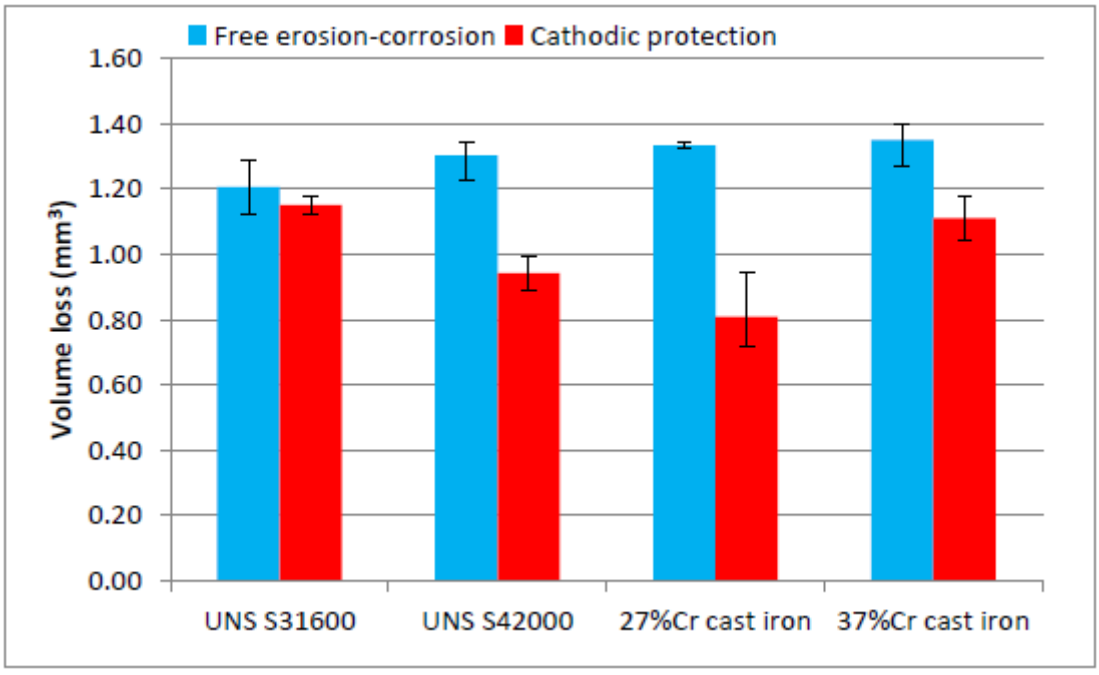

Figure 3: *Volume losses of the stainless steels and cast irons in free erosion corrosion and with cathodic protection*

3.3 Potentiodynamic polarisation scans

Figure 4 shows the anodic polarisation scans on the full specimen (38mm diameter) after 30 minutes of impingement. Periodic linear polarisation monitoring results (not shown herein) established that the corrosion rates were steady after this period. The normalised electrode potential (approximately 20mV below E_{corr}) has been employed for better comparison, since the E_{corr} values are different between the materials. The E_{corr} values are, however, presented in Table 5 which also shows the generated current densities from the Tafel extrapolations and the calculated mass losses via Faraday's law. It is apparent, from both Figure 3 and Table 6 that there are two groups of materials; the lower corrosion resistant materials (27%Cr cast iron and UNS S42000) and the more corrosion resistant materials (UNS S31600 and 37%Cr cast iron) whose corrosion rates are considerably lower than those of the martensitic-base materials.

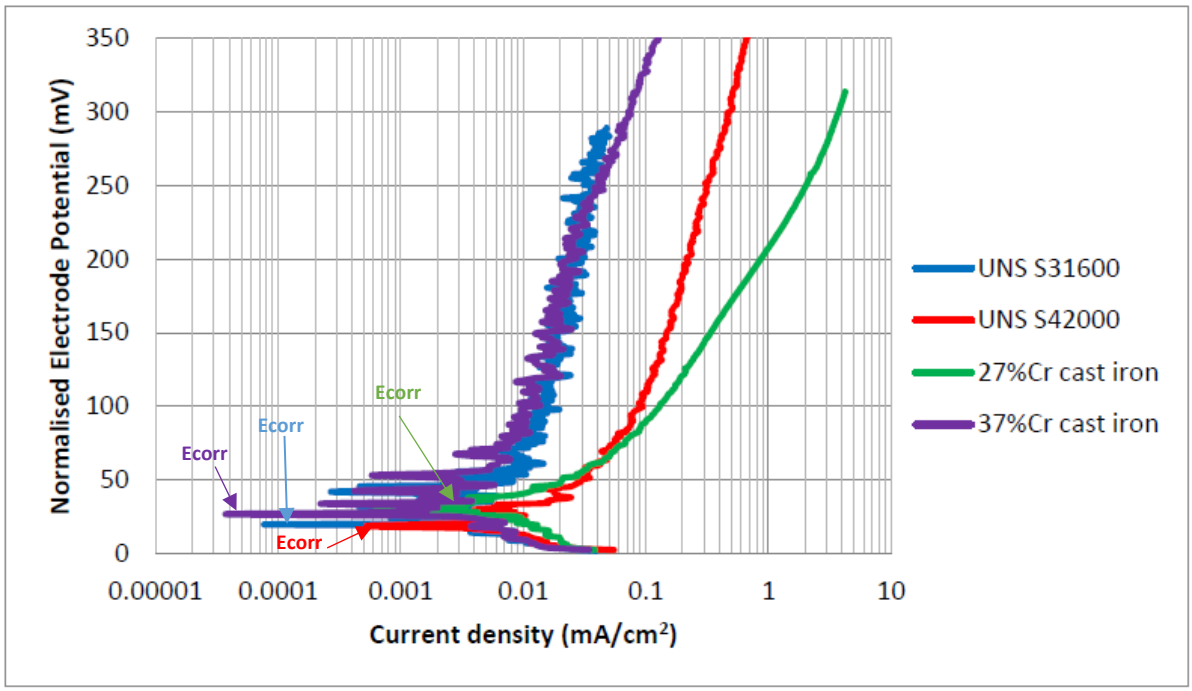

Figure 4: *Anodic polarisation scans on the full specimen of each comparator material in solid/liquid impingement*

Table 6: *Free corrosion potentials (E_{corr}), corrosion rates and calculated mass losses due to corrosion of the full specimen of each material*

Material	E_{corr} (mV)	Corrosion current density (mA/cm²)	Volume loss due to corrosion (mm³)
UNS S31600	-440	0.008	0.021
UNS S42000	-491	0.026	0.079
27%Cr cast iron	-471	0.035	0.107
37%Cr cast iron	-381	0.004	0.010

Figures 5-8 show the anodic polarisation results of each comparative material on the direct impinged zone and on the outer area of the segmented specimens, which gives greater detail of the corrosion behaviour of the materials in different hydrodynamic regimes. It is clear from these scans that the major difference between the two hydrodynamic zones is a substantial increase in the anodic reaction (and hence corrosion) rate in the more turbulent DIZ. Of course, in principle and as argued by others [30], the corrosion behaviour is also dependent upon the progress of the cathodic reaction but the consistently more negative values of E_{corr} in the DIZ compared to the outer region (Table 7) are indicative of the overriding role of anodic reactions in the severe flow conditions, associated with the high impingement velocities, prevalent in both zones in this investigation.

Table 7 lists the corrosion current densities along with the E_{corr} of each region through Tafel extrapolation by plotting a straight line from the average of the oscillating currents. The mass losses were calculated by using Faraday's law. A common attribute of all tested materials was that the corrosion current density on their direct impinged zone was considerably higher than that of their outer area.

In the outer region, the corrosion rates exhibited by UNS S42000 and 27%Cr cast iron are high and typical of actively corroding materials. The corrosion rates of the UNS S31600 and 37%Cr cast iron are much lower and represent alloys having a surface passive film. However, as Figures 5 and 8 demonstrate, the polarisation plots exhibit periodic current fluctuations that are indicative of de-passivation/re-passivation of a passive film. The observed fluctuations are typical for passive alloys experiencing slurry impingement conditions [13, 26, 27, 31].

In the DIZ, the corrosion current values exhibited by the UNS S31600 and 37%Cr cast iron are only 2 to 2.5 times less than those of UNS S42000 and 27%Cr because, under the severe solid particle impacts on the former, the de-passivation events are more severe than in the OA.

The overall ranking of the corrosion rates of the full specimen of the materials is in agreement with that of the segmented specimens as the austenitic-based alloys are exhibiting better corrosion resistance than the martensitic-based alloys.

.

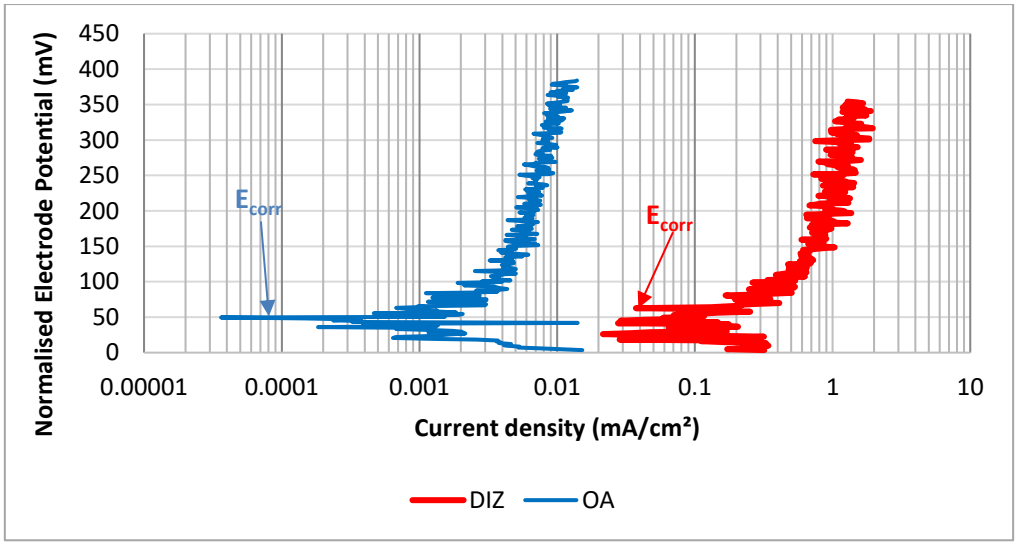

Figure 5: *Anodic polarisation scans on both segments of UNS S31600 in solid/liquid impingement*

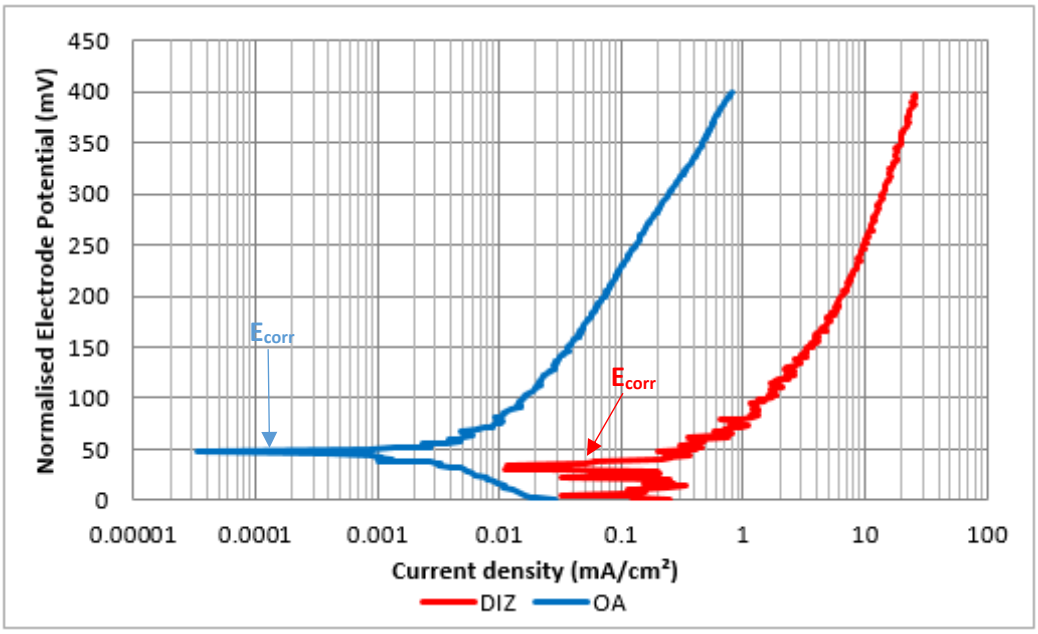

Figure 6: *Anodic polarisation scans on both segments of UNS S42000 in solid/liquid impingement*

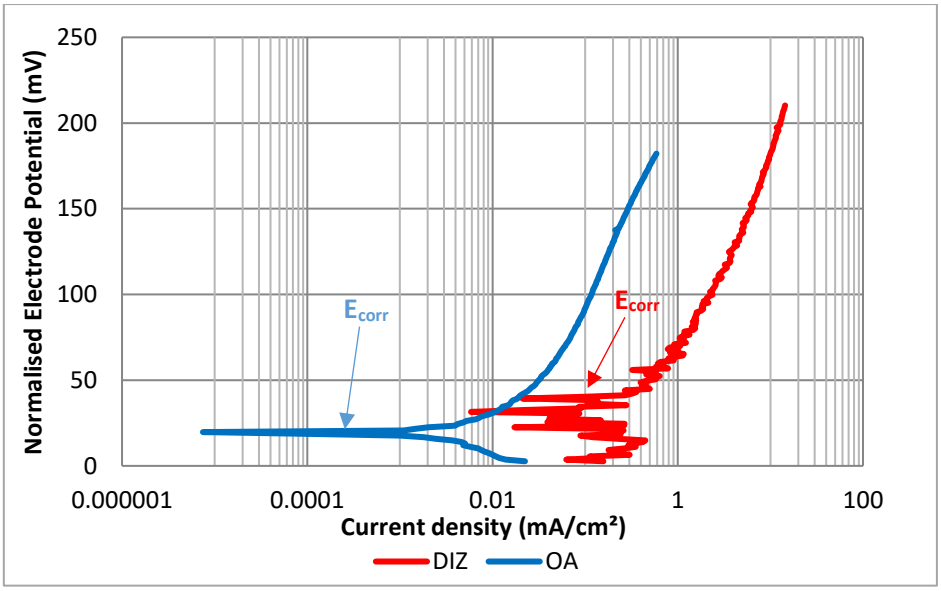

Figure 7: *Anodic polarisation scans on both segments of 27%Cr cast iron in solid/liquid impingement*

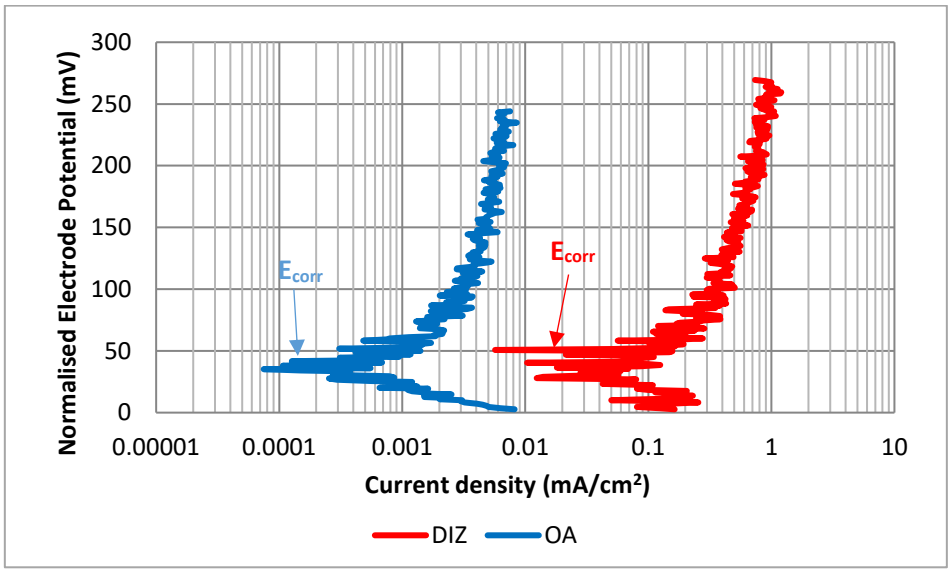

Figure 8: *Anodic polarisation scans on both segments of 37%Cr cast iron in solid/liquid impingement*

Table 7: *Free corrosion potentials (E_{corr}), corrosion rates and calculated mass losses due to corrosion on both areas of the segmented specimen*

Test Material	DIZ			OA		
	E_{corr} (mV)	Corrosion Current density (mA/cm²)	Volume loss due to corrosion (mm³)	E_{corr} (mV)	Corrosion Current density (mA/cm²)	Volume loss due to corrosion (mm³)
UNS S31600	-553	0.25	0.013	-369	0.002	0.005
UNS S42000	-563	0.50	0.025	-452	0.010	0.025

27%Cr cast iron	-529	0.50	0.027	-482	0.020	0.059
37%Cr cast iron	-531	0.20	0.008	-343	0.001	0.003

3.4 Post-test analysis

3.4.1 Wear damage under the jet

The deterioration processes occurring inside the wear scars was determined via SEM cross sections of the post-tested of both stainless steel and cast irons specimens and as in-plan views of the cast irons. The stainless steels exhibited different wear mechanisms than the high chromium cast irons. Figure 9 shows the cross section of the UNS S31600 stainless steel wear scar. It is evident that erosion-related deformation has taken place within the subsurface regions. The thickness of the UNS S31600 hardened layer is about 30μm. Such distorted surface structure was not evident in the region outside the wear scar of the austenitic stainless steel. On the other hand, a hardened layer was not apparent on the wear scar of UNS S42000 stainless steel.

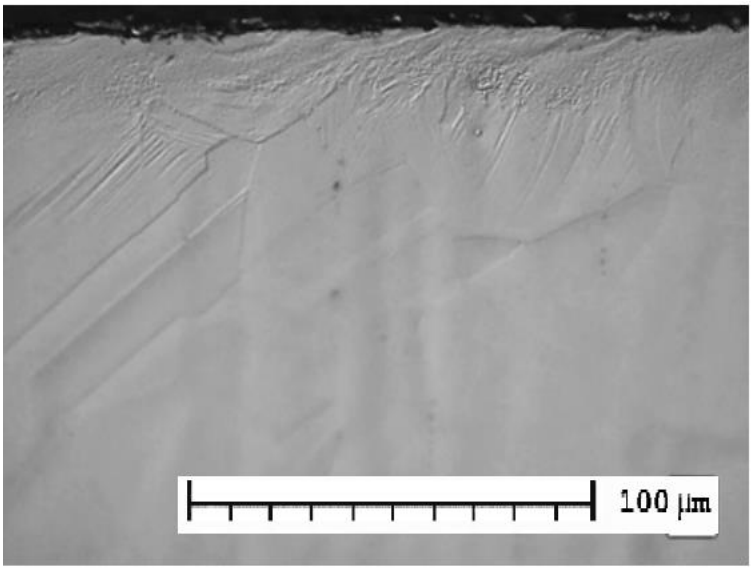

Figure 9: *Hardened layer on the UNS S31600 wear scar*

Many researchers [32–34] in the past have seen the strain hardening effect in erosion-corrosion conditions, and an increase in sub-surface hardness has been observed in another study [31]. Singh et al. [35], found that the surface hardening of the UNS S316000 was substantial, as the hardness was increased from 160HV_{50} to 430HV_{50} during air blast erosion at normal incidence. In the current study, Knoop hardness testing was employed to assess the intensity of hardness near the surface due to the impact stresses of the sand particles. Table 8 illustrates the average

of ten indentations parallel to the surface of the wear scar and in the core of the stainless steel, along with their standard deviation. It is evident that the near-surface hardness has been increased by almost 100HK by the impact effect of the particles.

Table 8: *Average hardness measurements and standard deviation on the hardened layer and the core material of the UNS S31600*

	Hardened layer (HK)	Core material (HK)
Average	248	147
Standard deviation	10	7

Figure 10A shows a plan view of the heavily degraded microstructure of the 27%Cr cast iron in the wear scar zone after solid/liquid impingement in FEC conditions. Extensive micro-cracking of the chromium carbides, with some spalling events, are apparent in the wear scar, as a result of the impact stresses of the striking erodent that cause fracture of the Cr_7C_3 rod-like carbides. On the other hand, the martensite, which surrounds the carbides, has been widely deformed as is also apparent on the martensitic stainless steel (Figure 11).

Figure 10B and C illustrates cross sections of the 27%Cr cast iron wear scar after testing in FEC conditions, where subsurface cracking is evident for at least 20μm below the surface. This feature demonstrates that the impact stresses of the abrasives have also been transmitted to the carbides and martensite, causing multiple cracks on the former while the latter deforms. The fracture of the carbides below the surface would lead to easier spalling on successive erodent impacts.

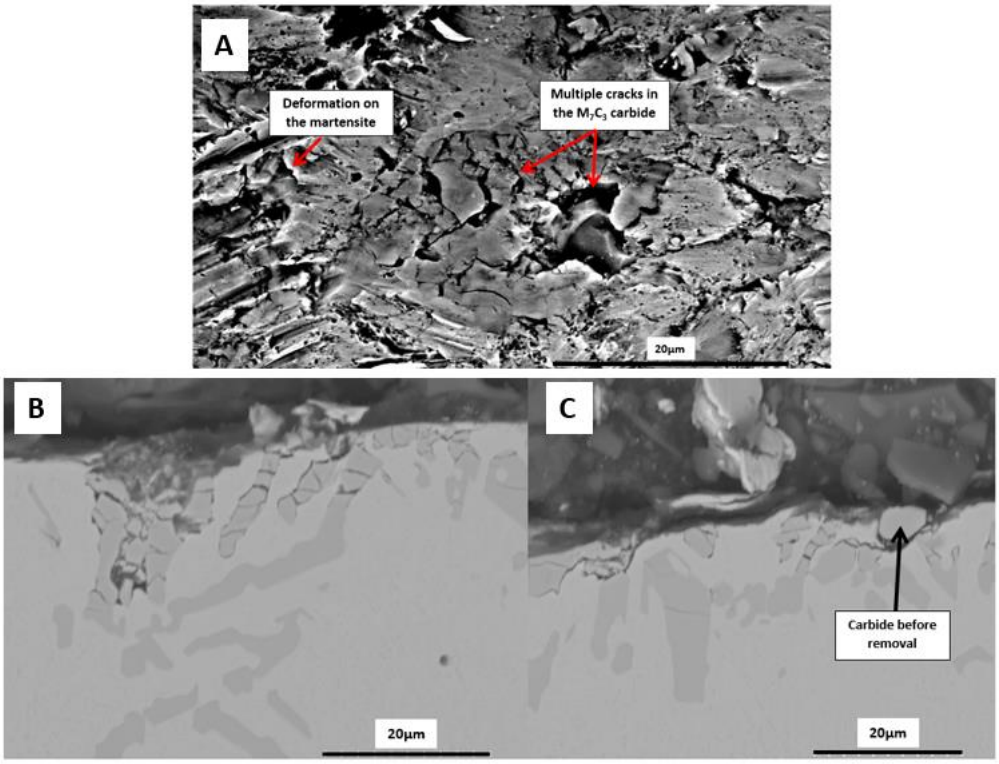

Figure 10: *A) Plan view of carbide cracking and spalling sites inside the wear scar of the 27%Cr cast iron; B) and C) cross sections of the 27%Cr cast iron wear scar with heavily cracked chromium carbides and carbide removal*

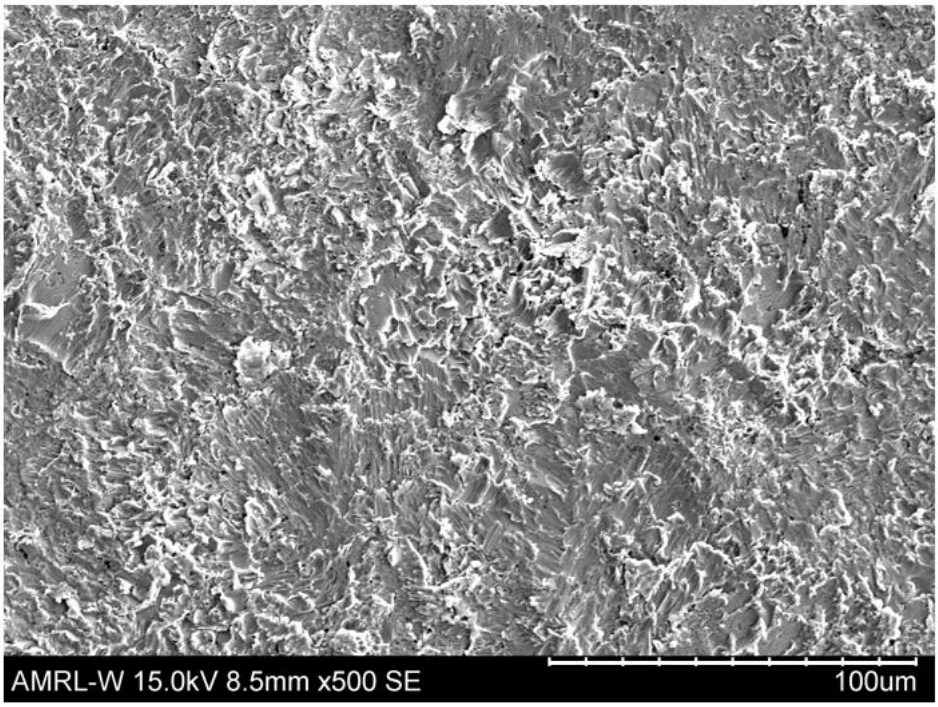

Figure 11: *Plan view of damage observed in wear scar of martensitic stainless steel*

Figure 12A illustrates, in-plan, the cracked eutectic carbides in the wear scar of the 37%Cr cast iron after solid/liquid impingement. Figure 12B and 11C show the cross sections of the 37%Cr cast iron wear scar, where extensive subsurface cracking had also taken place for at least 30µm below the top surface. This trait triggers the detachment of lumps of the cast irons which would include both austenite and eutectic carbides. It should be noted that the sub-surface cracking was not observed in regions of the cross sections outside the wear scar of both cast irons.

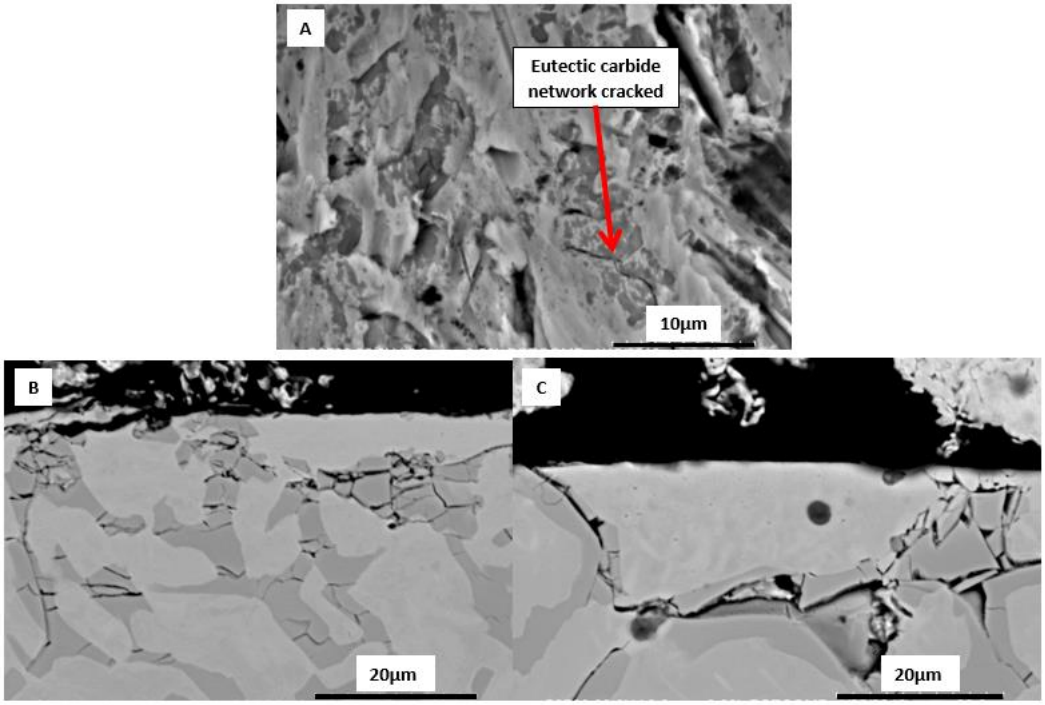

Figure 12: *A) Plan view of extensive cracking on the eutectic carbide network inside the wear scar of the 37%Cr alloy; B) and C): cross-sections showing b) Vertical and perpendicular cracking on the eutectic carbides; and C) Continuous cracking on chromium carbides below a segment of austenite*

3.4.2 Three- dimensional surface topography

Figure 13a shows the relatively uniform 3D profile of the 27%Cr cast iron wear scar, which is also typical of the stainless steels. However, the wear scar morphology observed in the 37%Cr cast iron, as illustrated in Figure 13b, exhibits an irregular shape with peaks and valleys in all impingement conditions (i.e. free erosion-corrosion and cathodic protection). This feature is a result of the distinct hardness difference between the matrix (251HV) and the eutectic structure (459HV) and the extensive cracking of the eutectic carbides shown in Figures 12a, b and c.

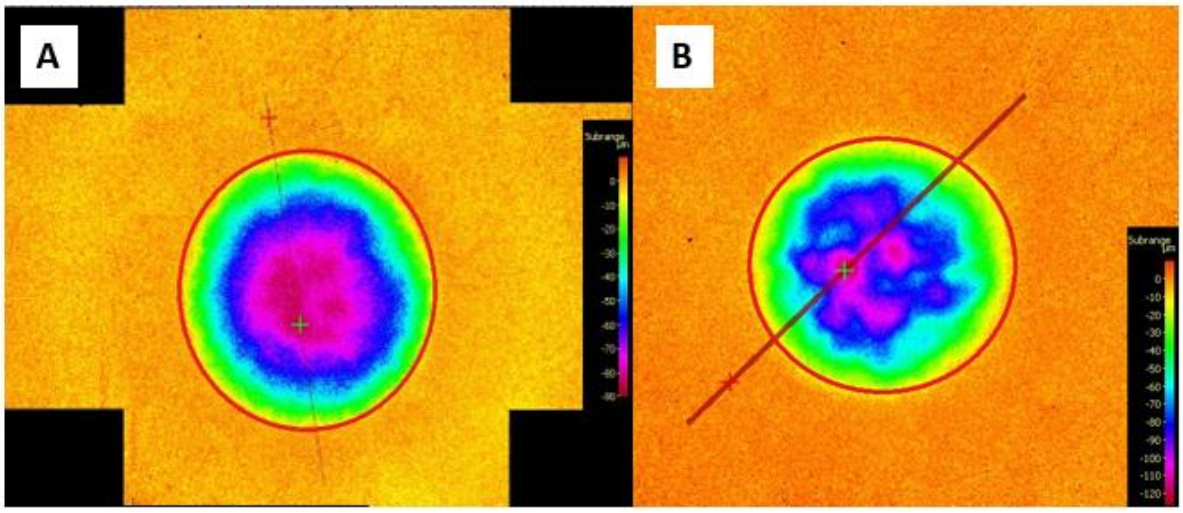

Figure 13: *Volumetric analysis measurement on the direct impinged zone after solid-liquid impingement a) 27%Cr cast iron; b) 37%Cr cast iron*

Surface profile scans were performed on the wear scar of each specimen to broaden the evaluation of the deterioration mechanisms occurring in the zone directly under the impinging jet. Figure 14a illustrates examples of the wear of the 27%Cr cast iron under free erosion-corrosion conditions and cathodic protection. The substantial effect of corrosion related damage is apparent on the wear scar profile scan on the martensitic-structured material. A similar observation was observed for the UNS S42000 stainless steel, Figure 14b. Figure 14c shows the wear scar profile scans of the 37%Cr cast iron under free erosion-corrosion conditions and cathodic protection. There is a clear difference in the wear scar depths under free erosion-corrosion conditions compared to the pure erosion conditions as observed on the martensitic-based alloys above, but the most interesting feature from this profile examination is the uneven shape of the wear scar in both conditions (see also Figure 13b) which indicates that the mechanical effect of sand particles have impacted differently upon the microstructure of the 37%Cr cast iron. For the UNS S31600 stainless steel, there was no significant difference in the two depths (Figure 14d), which indicates that the dominant degradation mechanism occurring in the UNS S31600 wear scar is erosion.

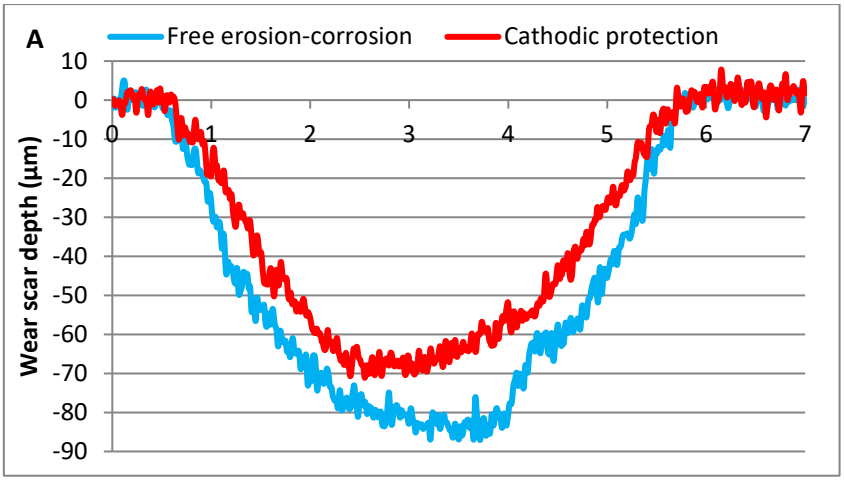
A
Free erosion-corrosion
Cathodic protection
Wear scar depth (µm)
10
0
-10
-20
-30
-40
-50
-60
-70
-80
-90
0
1
2
3
4
5
6
7

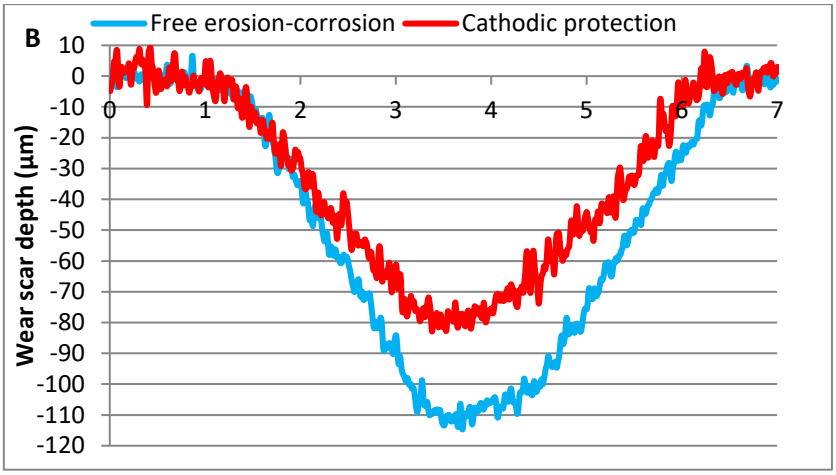
B
Free erosion-corrosion
Cathodic protection
Wear scar depth (µm)
10
0
-10
-20
-30
-40
-50
-60
-70
-80
-90
-100
-110
-120
0
1
2
3
4
5
6
7

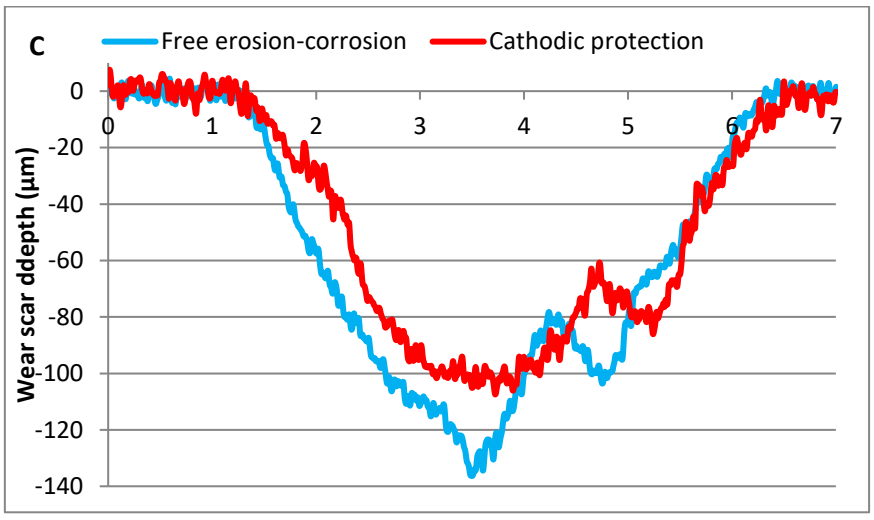
C
Free erosion-corrosion
Cathodic protection
Wear scar ddepth (µm)
0
-20
-40
-60
-80
-100
-120
-140
0
1
2
3
4
5
6
7

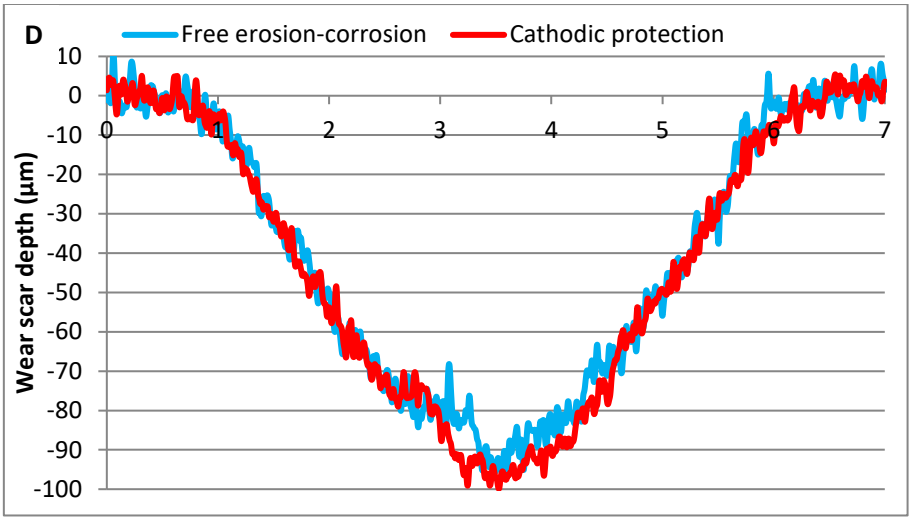

Figure 14: *Surface profile scans of the wear scars for the test materials in free erosion-corrosion and cathodic protection after solid/liquid impingement – a) 27%Cr cast iron; b) UNS S42000; c) 37%Cr cast iron; d) UNS S31600*

Figure 15 illustrates the volume losses of the comparative materials within the direct impinged zone during solid/liquid impingement with and without cathodic protection. The volume losses, when the cathodic protection was applied, were reduced. The UNS S31600 had about 5% reduction on the wear scar volume, whereas the UNS S42000 and both cast irons exhibited about 30% reduction which shows the benefit of cathodic protection on those materials. It is clear that the basis, of the relatively lower resistance to erosion corrosion exhibited by the cast irons, is their vulnerability to enhanced damage in circumstances when the pure mechanical damage is not overwhelming.

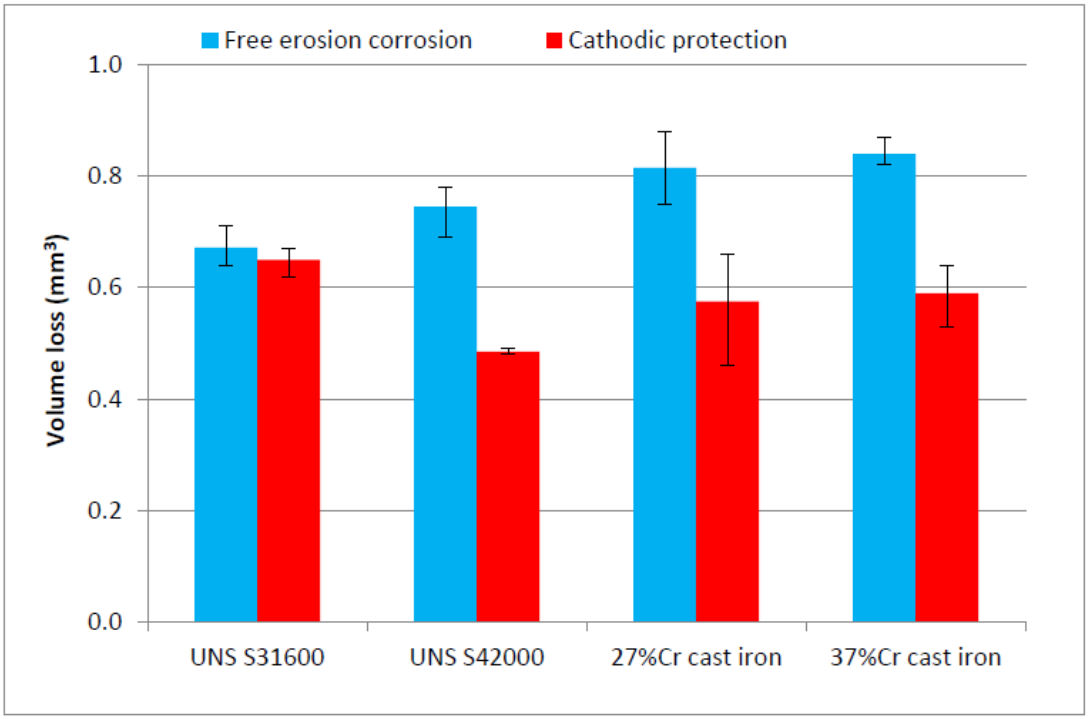

Figure 15: *Comparison of the average volume losses within the wear scar of the two stainless steels and the two cast irons with and without cathodic protection*

3.4.3 Volumetric analysis

The quantitative volume losses, shown in Figure 16, demonstrate the in-house developed enhanced volumetric analysis technique which has previously been reported [26]. The overall material loss due to erosion-corrosion can be broken down into the individual degradation processes which are detailed in equation (1) below.

$$TVL = E_{DIZ} + C_{DIZ} + S_{DIZ} + SA_{OA} + C_{OA} + S_{OA} \qquad (1)$$

Where, TVL is the total volume loss, E_{DIZ}, C_{DIZ} and S_{DIZ} are the high-angle erosion, corrosion and synergy occurring in the DIZ and SA_{OA}, C_{OA} and S_{OA} are the low-angle sliding abrasion, corrosion and synergy damage occurring in the OA.

When CP is applied the corrosion-related processes are eliminated, leaving only the mechanical damage mechanisms occurring in both regions, as demonstrated in the equation (2) below.

$$TVL_{CP} = E_{DIZ} + SA_{OA} \qquad (2)$$

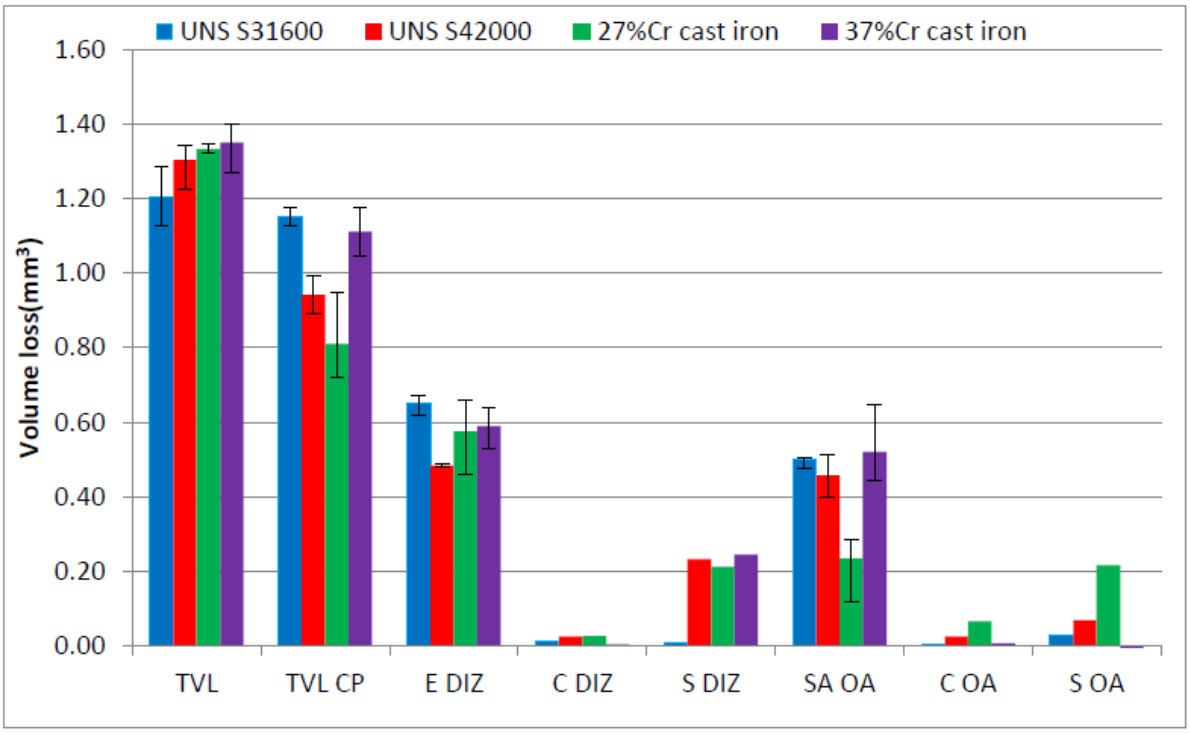

Figure 16: *Distinction of the different material degradation processes on the two stainless steels and the two cast irons*

4. Detailed discussion

4.1 Effect of cathodic protection

The employment of CP reduced the overall material loss of all materials. It is noteworthy, though, to mention that 27%Cr cast iron benefited the most by the application of CP, as its total volume loss was decreased by 39%. The UNS S42000 and 37%Cr cast iron also benefited from CP as their volume loss dropped by about 28% and 18%, respectively. On the other hand, the UNS S31600 volume loss fell by just 5%. This demonstrates that the corrosion related component, had the most substantial effect on the 27%Cr cast iron and the UNS S42000 and lower impact on the 37%Cr cast iron and the austenitic stainless steel. Similar traits, of the significant reduction of material loss with CP for the martensitic-based alloys and less of an effect for austenitic-based alloys due to their greater chromium matrix content, have been observed in previous studies [11, 17, 25].

4.2 Mechanisms

4.2.1 *Mechanical damage*

In terms of mechanical damage, the difference between the two stainless steels may be linked to their different hardness, even though the UNS S31600 was work hardened by the continuous

solid particle impact as shown in Figure 9. The relative behaviour of the two cast iron alloys is associated with their Cr/C ratio [11]. The 37%Cr cast iron exhibits a Cr/C ratio of 20.5 (Table 1) which is more than two times of the Cr/C ratio of the 27%Cr (9.0).

The material deterioration by erosion mechanisms that takes place inside the wear scar was determined by the volume loss analysis of the cathodically protected wear scars. The UNS S42000 showed the lowest erosion damage within the direct impinged zone. The two cast irons displayed higher volume loss than the martensitic stainless steel and this is attributed with the heavy cracking of their hard chromium carbides by the impinging particles, as observed in Figures 10 and 12. Nevertheless, both cast irons exhibited better erosion resistance in their wear scar than the austenitic stainless steel, which was the most vulnerable material under direct impingement erosion. According to the literature [1, 9, 15, 36], the hardness of a material cannot determine the erosion resistance of the material as a single factor, especially when the target exhibits a composite-like structure. Alternative correlations between mechanical properties and wear damage that have been suggested are the elastic modulus (E) and fracture toughness (K_{1c}) possibly in the form of a high hardness to elastic modulus ratio or a high H/K_{1C} ratio [37-39]. It is evident, however, that the aspect of appropriate correlations between material properties and wear mechanisms is still open to debate and it could be argued that, particularly in relation to high-velocity impingement, such correlations require employing mechanical properties measured under high strain rate conditions – which are, however, extremely sparse.

Comparing the damage in the direct impinged zone of the 37%Cr cast iron and the other test materials, the morphology of their wear scars were distinctly different as the 37%Cr cast iron had an asymmetrical wear scar and not a perfect U-shape as with the other three materials. It is evident that the soft austenitic dendrites of the 37%Cr cast iron, that comprise about 57% volume fraction of the overall structure, are selectively eroded and the protruding chromium carbides are susceptible to cracking and consequently spalling. Another interesting feature, though, was apparent on the cross sections of the 37%Cr cast iron wear scar (Figure 12) where the crack propagation on the eutectic carbides follows the eutectic structure that encloses the austenitic dendrites resulting in spalling of carbides and the large dendrites. This attribute has caused the uneven shape of the 37%Cr wear scar. On the other hand, the 27%Cr cast iron showed a different erosion mechanism as the rod-like carbides experienced cracking but the hard martensitic matrix was not eroded preferentially to the carbides; as a result, the mechanical support to the carbides was maintained.

In the experimental set up utilised in this research, the abrasion damage, in the outer zone, is, in a sense, an impingement at oblique angle. According to Finnie [36], the most vulnerable materials in low angle impingement are soft/ductile metals. In other words, the abrasion resistance of a material is dependant of the target material hardness. Thus, the two low hardness stainless steels were prone to sliding abrasion damage. On the other hand, the 27%Cr cast iron, as a less ductile cast iron with high volume fraction of rod-shape large chromium carbides and a hard martensitic matrix, exhibited superior sliding abrasion resistance. This links with the notion that high CVF often provides good durability to abrasion [2, 11, 40]. The hypoeutectic 37%Cr cast iron exhibited similar sliding abrasion resistance as the stainless steels, which could be associated with the low carbide volume fraction with small size eutectic chromium carbides (100 times smaller than the erodent) and also the soft austenitic dendrites. These microstructural features of the 37%Cr cast iron contributed to the relatively lower sliding abrasion resistance than the 27%Cr cast iron.

4.2.2 *Pure corrosion damage*

Although the volume loss due to pure corrosion within the wear scar and outer area, as calculated through Faraday's Law, was a small proportion of the overall damage for all comparative materials in this study, there were some differences in the corrosion rates. In the wear scar, the in-situ corrosion rates in Table 6 showed that the 27%Cr cast iron and the UNS S42000 corrosion rates were almost double that of the UNS S31600 and 2.5 times greater than the 37%Cr cast iron. In the outer area, the 37%Cr cast iron was two times better than the UNS S31600 (because of more Cr in the metal matrix of the 37%Cr cast iron), and the UNS S42000 was two times better than the 27%Cr cast iron. It is apparent that the chromium content in the matrix of the cast iron dictates their corrosion resistance, as suggested in the literature [10, 11, 14, 15, 41]. As shown in Table 3, the 37%Cr cast iron has almost 61% more chromium in the matrix compared to the 27%Cr cast iron, which has resulted in the observed difference in their corrosion behaviour.

4.2.3 *Synergy*

The extent of the enhancement of erosion by the corrosion (i.e. synergy) on the directly impinged zone was determined by the subtraction of the corrosion and erosion damage from the total volume loss in the direct impinged zone. Similarly, the synergy was quantified for the outer area with the respective outer area volumes. Synergy was a key factor of the material loss inside the wear scar of the two cast irons and the UNS S42000 but had a lower influence in the outer area. Synergy (S) was observed to be more predominant than pure corrosion (C) for both

wear regions. In the DIZ, the synergy values of the cast irons and the martensitic stainless steel were about eight times larger than the UNS S31600 but the differences were smaller in the outer area. Toro et al. [42] have suggested that intergranular corrosion along with uniform corrosion of the metallic matrix are the main mechanisms that enhance the mechanical removal of the martensitic stainless steel. However, it is considered that the major feature of the synergy of the two cast irons is interphase corrosion [13–17, 41] involving the different phases, chromium carbides and alloy matrix, present in the CCIs. It has been suggested [15] that this involves crevice corrosion but it is considered by the present authors that micro-galvanic interactions are more likely. Galvanic corrosion between two constituents in electrical contact occurs when the separate substances exhibit different electrode potentials. Studies have been carried out [16-20] in which the two phases, chromium carbide and ferrous alloy present in WCIs have been separated to facilitate measurement of the separate electrode potentials. These investigations have demonstrated that, in the aqueous conditions, saline water of around neutral pH, [17, 19, 20] carbides are noble to the alloy matrix. Thus, on account of the different electrode potentials of the carbides and metal matrix, the galvanic corrosion of the alloy phase results in weakening the interphase bond. This reduces the mechanical support for the carbides, thereby, facilitating their dislodgment causing additional material loss by mechanical action under the impingement conditions. In these hypoeutectic CCIs, such synergisitic action occurs within the eutectic colonies and involves different phases in the two cast irons:-

- M_7C_3 carbides and martensite in the 27%Cr alloy
- $M_{23}C_6$ carbides and austenite in the 37%Cr alloy

and the resulting galvanic currents would be expected to be different in the two materials – as argued below.

A major factor governing the magnitude of galvanic currents is the difference in the electrode potentials of the two components of the galvanic couple – the larger this is, the greater the galvanic current. If it is assumed that the electrode potential of the two types carbide are reasonably similar, then the magnitude of the driving potential difference will be determined by the electrode potentials of the alloy constituents. Now Fe-Cr alloys are often characterised by the spontaneous formation of a passive film on the surface and the electrode potential displayed by such an alloy is critically controlled by the presence of – or absence of – such a film which is a function of whether the alloy is in the active or passive state. Reference to the

electrochemical monitoring results on the segmented specimens (Figures 5-8) and to the summary table (Table 6) reveals the following:-

- In the outer region of the specimens (OA), the electrode potentials of the austenitic alloys are considerably less negative than those exhibited by the martensitic alloys. This implies that a passive film is a feature of the surface constitution on the austenitic alloy and this is demonstrated by the substantially-lower corrosion rates 20 times less) experienced by the 37%Cr iron in comparison with the 27%Cr alloy. These differences are associated (see Table 6) with the much higher chromium contents of the austenite phase in the 37%Cr cast iron than in the martensite constituent of the 27%Cr alloy. These features result in a much reduced driving force for galvanic corrosion in the 37%Cr material compared with the 27%Cr alloy and accounts for the significant degree of synergy in the martensitic alloy but virtual absence of synergy in the OA of the austenitic cast iron – see Figure 16.
- In the DIZ, however, the electrode potentials are very similar for all test materials and the corrosion rates of the high-alloy materials (UN31600 and 37%Cr cast iron) are only slightly less than for the martensitic alloys. This is attributable to the extremely severe impingement conditions present in the DIZ which restrict the ability to produce stable passive films on the austenitic alloys – resulting in much higher corrosion rates experienced by the austenitic alloys in the DIZ compared with the outer region (Figures 4 and 7). From the perspective of galvanic corrosion, therefore, the driving forces will be very similar in all the alloys investigated – leading to similar degrees of synergy in the DIZ (Figure 16).

The findings in this study illustrate the difficulties in predicting the relative behaviour of different materials in erosion corrosion situations where the corrosion element is not negligible. This complication is likely to be particularly prevalent in materials with a “metal matrix composite type of structure” that may be ascribed to CCIs. The complexity arises on account of the role of synergy – which is often [17] found to represent a substantial proportion of the total material loss especially in erosion corrosion circumstances which are not erosion dominated. Whilst the magnitude of the pure corrosion attack may be relatively minor, the corrosion conditions can drive micro-galvanic corrosion (and hence synergy) to high extents. Thus, predicting the amounts of synergy contribution is non-trivial – especially when, as demonstrated in this investigation, these corrosion/mechanical interactions can be very dependent upon the effectiveness of passivation and especially on the local hydrodynamic

condition. A further complicating factor arises from potential variations in the relative nobilities of carbide phase and alloy matrix; for these CCIs this appears [17-20] to be dependent upon the water chemistry – with evidence, for instance, of carbides being less noble than the alloy in water of high pH. A further relevant factor is the area ratio effect on galvanic currents. This has not been an issue in the present work because the micro-galvanic actions were occurring in a eutectic matrix but if, as in the case of hypereutectic CCIs, there are primary carbides present, the synergy effects will be further complicated by two types of galvanic interaction – those associated with the coarse carbides and those in the eutectic mixture. The influence of area ratio may become important in determining the magnitude of galvanic currents in the former location and this, in turn, would be expected to be influenced by the geometric dispersion of the primary carbide phase. All in all, these difficulties in predicting and controlling the type and extent of these corrosion/mechanical interactions perhaps provide an impetus towards consideration of cathodic protection as a means of stifling all corrosion-induced material loss in corrosive wear situations in electrochemically-aggressive industrial environments. It is recognised, however, that there will be serious design issues associated with the application of CP in many of the components for which CCIs are commonly employed.

5. Conclusions

1. The experimental protocol adopted yielded more detailed discrimination of the various degradation mechanisms that take place during erosion-corrosion. This feature would not be perceptible by only considering the total volume loss (i.e. on a single specimen). The differing degrees of damage occurring in the high-angle directly-impinged zone and the low-angle outer regions, implies that optimal material selection is required for these two different hydrodynamic conditions.
2. In the corrosive conditions studied, no discernible distinctions, between the materials investigated, were evident in the free erosion-corrosion performances. The application of CP, however, revealed differences between the materials in the pure mechanical conditions. Overall, the two martensitic alloys displayed lower pure mechanical damage than the austenitic alloys but, when the behaviour in the two distinct hydrodynamic zones was considered, it became evident that the superior performance of the 27%Cr cast iron occurred in the outer region and was associated with a higher resistance to abrasive damage promoted by its high concentration of hard carbides. The martensitic stainless steel displayed greater relative resistance to pure mechanical damage than the 27%Cr cast iron in the directly impinged zone because the carbides

are prone (Figures 10, 12) to cracking by direct impingement. The differences in resistance to direct impingement damage between the two stainless steels are less clear but are likely to be associated with the higher hardness of the martensitic alloy.

3. In relation to the martensitic-structured materials, the chromium carbides within the hard martensitic matrix of the 27%Cr cast iron provided superior resistance to sliding abrasion but, under direct impingement, the carbides cracked making the 27%Cr CCI less erosion resistant than the UNS 42000 steel. The lower chromium concentrations in the martensitic-structured materials caused these alloys to undergo relatively high corrosion rates.
4. The main differences between the behaviour of the 37%Cr cast iron and the UNS S31600 stainless steel were that the corrosion-related component of the 37%Cr cast iron is higher than UNS S31600 in the direct impinged zone due to the interaction of the metallic matrix with the carbides. On the other hand, the 37%Cr cast iron exhibited superior corrosion resistance in the outer area due to the higher Cr content of this CCI.
5. Comparing the two cast irons, it is evident that the 27%Cr cast iron has superior resistance to low-angle abrasion but not to direct impingement erosion. In terms of corrosion-related damage, the value of increased chromium in the 37%Cr cast iron is only obtained in low-angle conditions (where the corrosion component of damage is significant) and does not extend to high-angle erosion-corrosion situations on account of the predominance of erosive damage in this zone. For the latter circumstances, a better strategy might be to employ a lower-chromium cast iron (e.g. 27%Cr) in combination with cathodic protection.
6. The main influence of a corrosive environment is in increasing the synergy rather than the pure corrosive attack. This factor arises on account of micro-galvanic interactions at interphase boundaries and demonstrates the crucial need to consider interactions between mechanical and electrochemical damage during assessment of erosion corrosion behaviour. The substantial role of synergy in the overall damage of two-phase materials poses particular problems in optimising the composition and microstructure of white cast irons and also probably for other metal-matrix composites.

Acknowledgments

The authors would like to acknowledge the support for this study, which was provided by the Weir Group PLC (WARC2011- SAA1, 2011) via its establishment of the Weir Advanced Research Centre (WARC) at the University of Strathclyde.

References

[1] R. J. Chung, X. Tang, D. Y. Li, B. Hinckley, and K. Dolman, "Abnormal erosion-slurry velocity relationship of high chromium cast iron with high carbon concentrations", *Wear*, vol. 271, no. 9–10, pp. 1454–1461, 2011.

[2] J. K. Fulcher, T. H. Kosel, and N. F. Fiore, "The effect of carbide volume fraction on the low stress abrasion resistance of high Cr-Mo white cast irons", *Wear*, vol. 84, no. 3, pp. 313–325, 1983.

[3] B. Lu, J. Luo, and S. Chiovelli, "Corrosion and wear resistance of chrome white irons - A correlation to their composition and microstructure", *Metall. Mater. Trans. A Phys. Metall. Mater. Sci.*, vol. 37, no. 10, pp. 3029–3038, 2006.

[4] M. M. Arikan, H. Cimenoğlu, and E. S. Kayali, "The effect of titanium on the abrasion resistance of 15Cr-3Mo white cast iron", *Wear*, vol. 247, no. 2, pp. 231–235, 2001.

[5] R. J. Chung, X. Tang, D. Y. Li, B. Hinckley, and K. Dolman, "Effects of titanium addition on microstructure and wear resistance of hypereutectic high chromium cast iron Fe-25wt.%Cr-4wt.%C", *Wear*, vol. 267, no. 1–4, pp. 356–361, 2009.

[6] H.-X. Chen, Z.-C. Chang, J.-C. Lu, and H.-T. Lin, "Effect of niobium on wear resistance of 15%Cr white cast iron", *Wear*, vol. 166, no. 2, pp. 197–201, 1993.

[7] R. J. Chung, X. Tang, D. Y. Li, B. Hinckley, and K. Dolman, "Microstructure refinement of hypereutectic high Cr cast irons using hard carbide-forming elements for improved wear resistance", *Wear*, vol. 301, no. 1–2, pp. 695–706, 2013.

[8] Y. P. Wang, D. Y. Li, L. Parent, and H. Tian, "Performances of hybrid high-entropy high-Cr cast irons during sliding wear and air-jet solid-particle erosion", *Wear*, vol. 301, no. 1–2, pp. 390–397, 2013.

[9] S. G. Sapate and A. V. Rama Rao, "Effect of carbide volume fraction on erosive wear behaviour of hardfacing cast irons", *Wear*, vol. 256, no. 7–8, pp. 774–786, 2004.

[10] X. H. Tang, R. Chung, C. J. Pang, D. Y. Li, B. Hinckley, and K. Dolman, "Microstructure of high (45wt.%) chromium cast irons and their resistances to wear and corrosion", *Wear*, vol. 271, no. 9–10, pp. 1426–1431, 2011.

[11] M. Jones and R. J. Llewellyn, "Erosion-corrosion assessment of materials for use in

the resources industry", *Wear*, vol. 267, no. 11, pp. 2003–2009, 2009.

[12] H. H. Tian, G. R. Addie, and R. J. Visintainer, "Erosion-corrosion performance of high-Cr cast iron alloys in flowing liquid-solid slurries", *Wear*, vol. 267, no. 11, pp. 2039–2047, 2009.

[13] G. Karafyllias, A. Galloway, and E. Humphries, "The effect of low pH in erosion-corrosion resistance of high chromium cast irons and stainless steels", *Wear*, vol. 420–421, no. March 2018, pp. 79–86, 2019.

[14] A. Neville, F. Reza, S. Chiovelli, and T. Revega, "Characterization and corrosion behavior of high-chromium white cast irons", *Metall. Mater. Trans. A Phys. Metall. Mater. Sci.*, vol. 37, no. 8, pp. 2339–2347, 2006.

[15] A. Neville and F. Reza, "Erosion-corrosion of cast white irons for application in the oilsand industry," in *NACE International Corrosion EXPO. 2007*, 2007, Paper No. 07678.

[16] S. W. Watson, B. W. Madsen, and S. D. Cramer, "Wear-corrosion study of white cast irons", *Wear*, vol. 181–183, pp. 469–475, 1995.

[17] A. F. Zhang, J. D. Xing, L. Fang, and J. Y. Su, "Inter-phase corrosion of chromium white cast irons in dynamic state", *Wear*, vol. 257, no. 1–2, pp. 198–204, 2004.

[18] M. Salasi, G. B. Stachowiak, and G. W. Stachowiak, "Three-body tribocorrosion of high-chromium cast irons in neutral and alkaline environments," *Wear*, vol. 271, no. 9–10, pp. 1385–1396, 2011.

[19] V. Marimuthu, K. Kannoorpatti, "Corrosion behaviour of high chromium white iron hardfacing alloys in acidic and neutral solutions", *J Bio Tribo Corros,* vol. 2, Article no. 29, 2016.

[20] V. Marimuthu, I. Dulac, K. Kannoorpatti "Significance of Pourbaix Diagrams to Study the Corrosion Behaviour of Hardfacing Alloys Based on Chromium Carbides at 298 K (25 °C)", *J Bio Tribo Corros*, vol. 2, Article no. 17, (2016)

[21] R. J. Llewellyn, S. K. Yick, and K. F. Dolman, "Scouring erosion resistance of metallic materials used in slurry pump service", *Wear*, vol. 256, no. 6, pp. 592–599, 2004.

[22] Y. Xie, J. Jiang, K. Y. Tufa, and S. Yick, "Wear resistance of materials used for slurry transport", *Wear*, vol. 332–333, pp. 1104–1110, 2015.

[23] A. N. J. Stevenson and I. M. Hutchings, "Wear of Hardfacing While Cast Irons By Solid Particle Erosion", *Wear*, vol. 186, no. 1, pp. 150–158, 1995.

[24] M. A. Al-Bukhaiti, S. M. Ahmed, F. M. F. Badran, and K. M. Emara, "Effect of

impingement angle on slurry erosion behaviour and mechanisms of 1017 steel and high-chromium white cast iron", *Wear*, vol. 262, no. 9–10, pp. 1187–1198, 2007.

[25] G. Karafyllias, L. Giourntas, T. Hodgkiess, and A. M. Galloway, "Relative performance of two cast irons and two stainless steels under erosion-corrosion conditions", in *Nace International Corrosion Expo. 2016*, 2016, Article no. 7723.

[26] L. Giourntas, T. Hodgkiess, and A. M. Galloway, "Enhanced approach of assessing the corrosive wear of engineering materials under impingement", *Wear*, vol. 338–339, pp. 155–163, 2015.

[27] F. Brownlie, C. Anene, T. Hodgkiess, A. Pearson, and A. M. Galloway, "Comparison of Hot Wire TIG Stellite 6 weld cladding and lost wax cast Stellite 6 under corrosive wear conditions", *Wear*, vol. 404–405, 2018.

[28] G. Karafyllias, "The effect of acidity and salinity level in erosion-corrosion performance of metals" Ph.D thesis, University of Strathclyde, Glasgow, 2017.

[29] R. Chattopadhyay, *Surface Wear: Analysis, Treatment and Prevention*. Novelty, Ohio, USA, ASM International, 2001.

[30] M. Walczak, S. Sharifi, M. M. Stack, "On a multiphysics approach to modelling erosion-enhanced corrosion of low-alloy carbon steel in chloride containing environments", *Corrosion Science*, 176, 2020, Paper no. 109045.

[31] S. Aribo, R. Barker, X. Hu and A. Neville " Erosion-corrosion behaviour of lean duplex stainless steels in 3.5% NaCl solution", *Wear,* vol. 302, pp. 1602-1608, 2013.

[32] I. M. Hutchings and P. H. Shipway, *Tribology: Friction and wear of engineering materials*. Oxford, UK, Elsevier Ltd, 2017.

[33] R. J. K. Wood, J. C. Walker, T. J. Harvey, S. Wang, and S. S. Rajahram, "Influence of microstructure on the erosion and erosion-corrosion characteristics of 316 stainless steel", *Wear*, vol. 306, no. 1–2, pp. 254–262, 2013.

[34] T. A. Adler and Ö. N. Doğan, "Damage by indentation and single impact of hard particles on a high chromium white cast iron", *Wear*, vol. 203–204, pp. 257–266, 1997.

[35] T. Singh, S. N. Tiwari, and G. Sundararajan, "Room temperature erosion behaviour of 304, 316 and 410 stainless steels", *Wear*, vol. 145, no. 1, pp. 77–100, 1991.

[36] I. Finnie, "The mechanism of erosion of ductile metals," in *3rd U.S. Congr. Appl. Mechanics*, 1958.

[37] Y. Ben-Ami, A. Uzi, A. Levy, "Modelling the particles impingement angle to produce maximum erosion", *Powder Technology*, 301, pp. 1032-1043, 2016.

[38] A. R. Chinta, K. Valtonen, V. T. Kuokkala, S. Kundu, M. J. Peet, H. K. D. H. Bhadeshia, "Role of fracture toughness in impact abrasion wear", *Wear*, 428-429, pp. 430-437, 2019.

[39] A. Leyland, A. Matthews, "On the significance of the H/E ratio in wear control: a nanocomposite coating approach to optimised tribological behaviour", *Wear,* 246 (1-2), pp. 1-11, 2000.

[40] K. Zum Gahr and G. T. Eldis, “Abrasive Wear of White Cast Irons”, *Wear*, vol. 64, no. 1, pp. 175–194, 1980.

[41] H. H. Tian and P. A. Taylor, “Corrosion study on high alloyed white cast irons in acidic and chloride containing solutions,” in *NACE International corrosion Expo 2011*, 2011, Article no. 11250.

[42] A. Toro, A. Sinatora, D. K. Tanaka, and A. P. Tschiptschin, “Corrosion-erosion of nitrogen bearing martensitic stainless steels in seawater-quartz slurry”, *Wear*, vol. 251, pp. 1257–1264, 2001.